Explaining the flat-spectrum radio core Sgr A* with GRMHD simulations of jets

Monika A. Mościbrodzka

Department of Astrophysics/IMAPP, Radboud University
P.O. Box 9010, 6500 GL Nijmegen, The Netherlands
email: m.moscibrodzka@astro.ru.nl

Abstract. The supermassive black hole in the center of the Milky Way, Sgr A*, displays a nearly flat radio spectrum which is typical for jets in Active Galactic Nuclei. Indeed, time dependent, magnetized models of radiatively inefficient accretion flows, which are commonly used to explain the millimeter, near-infrared, and X-ray emission of Sgr A* also often produce jet-like outflows. However, the emission from these models so far has failed to reproduce the flat radio spectrum. We show that current GRMHD simulations can naturally reproduce the flat spectrum, when using a two-temperature plasma in the disk and a constant electron temperature plasma in the jet. This assumption is consistent with current state-of-the art simulations, in which the electron temperature evolution is not explicitly modeled. Stronger magnetization and stronger shearing seen in the jet sheath could possibly explain the difference in electron heating between jet and disk. The model images and spectra are consistent with the radio sizes and spectrum of Sgr A*.

Keywords. accretion, accretion disks, black hole physics, MHD, radiative transfer, relativity, Galaxy: center

1. Introduction

The very center of the Milky Way host a compact, nearly flat spectrum ($\alpha_\nu \approx 0.3$) radio source referred to as Sgr A*. The radio object coincides with the location of the central supermassive object (possibly a supermassive black hole, Falcke & Markoff 2013) but its intrinsic structure/geometry is washed out by the scattering effects of the interstellar medium electrons (Bower *et al.* 2006, Bower *et al.* 2014). What is then the origin of the bright ($F_{1-690GHz} \sim 1$ Jy) radio emission? Currently, two theories are under the debate. Using various assumptions the nearly flat radio spectrum can be displayed by a relativistic jet or by a relativistically hot, magnetized accretion flow onto the supermassive black hole. Recently, it became possible to directly probe the intrinsic source geometry by using the Event Horizon Telescope (EHT, Doeleman *et al.* 2008). Hence, there is a possibility to test the two theories.

EHT is a millimeter Very Long Baseline Interferometry (VLBI) experiment to observe Sgr A* (and the core of M87 galaxy) at $\lambda = 1.3$ and 0.87 mm (Doeleman *et al.* 2008, Doeleman *et al.* 2012). At these wavelengths the Galactic electron scattering attenuates and in principle sharp images of the source could be constructed. Also, around sub-mm the source itself becomes optically thin, so the EHT promises to image the horizon silhouette of the supermassive black hole. Unfortunately, due to low number of mm-VLBI stations used the image reconstruction is not available yet. One can still compare the model images by modeling the VLBI observables, like visibility function, based on the synthetic intensity maps. In this proceeding, we present which models are consistent with the current observations. The currently available visibility data already put strong constraints on the theoretical models. Here, we also briefly discuss how to probe the

374
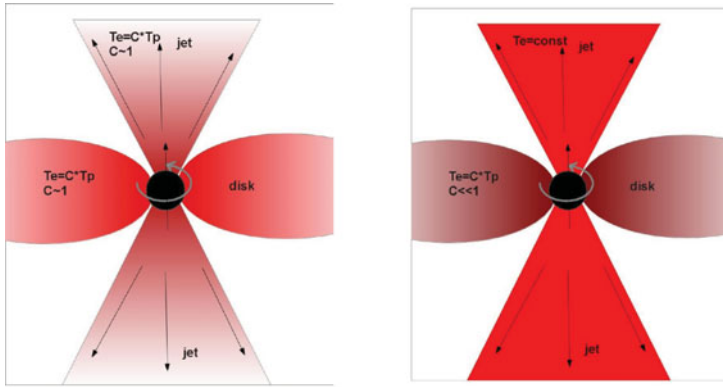
Figure 1. Diagrams show two geometrical models for the electron temperature in the GRMHD simulations of accreting black hole. The left panel displays the single temperature model in which electrons are strongly coupled to the protons. In the right panel, the electrons are weakly coupled to protons in the accretion disk and they have constant temperature along the jet.

source intrinsic geometry at longer wavelengths $\lambda = 3.5$ mm at which the interstellar medium electron scattering becomes dominant.

2. Testing models of accreting supermassive black hole

We test three dimensional General Relativistic Magnetohydrodynamics (GRMHD) simulations of magnetized gas around a supermassive, spinning black hole (the dimensionless spin of the black hole is $a_* \approx 0.94$). Our model extends from the black hole horizon to radius of 240 R_g (where $R_g = GM_{BH}/c^2$) which corresponds to size of 20AU when model is scaled to Sgr A* system or 2.4 mas on the sky, if the same model is placed at a distance of 8.5 kpc. In the considered simulation, a magnetized jets are naturally produced by magnetic forces and the spinning black hole. It is worth mentioning that the jets have two components: spine and sheath. Spine of the jet is strongly magnetized and has low matter content. The jet sheath is a thin layer of outflowing gas surrounding the nearly empty spine. Any electromagnetic emission produced in the jet will be dominated by the sheath due to its higher, compared to spine, matter content. Next, a general relativistic radiative transfer numerical scheme is used to compute post-processing, synthetic spectra and synchrotron emission maps of the plasma as observed on the Earth. Our goal is to simultaneously reproduce Sgr A* observed spectral energy distribution and its size in the radio band. For further details of our calculations see Mościbrodzka *et al.* (2014).

In our radiative transfer model all variables, but one, necessary to compute the synchrotron emissivities and absorptivities, are taken directly from the GRMHD run. The variable that is not yet explicitly modeled in the GRMHD simulation is the electron temperature, T_e. In principle in the slowly accreting systems, such as Sgr A*, the plasma is collisionless and electron distribution function may vary from the proton one that governs the MHD equations. Since synchrotron radiation is produced by electrons, the uncertain prescription for the T_e leaves us a lot of degrees of freedom in the radiation modeling.

In this work, we investigate two simplified geometrical models for T_e distributions (schematic diagrams are shown in Fig. 1). In the first prescription (left panel in Fig. 1), we assume that electrons are always coupled to protons, regardless if they are in the turbulent disk or magnetic jet. The coupling constant is of the order of unity, $C \equiv T_p/T_e = 1$. This model has been previously explored by other authors (e.g., Noble *et al.*
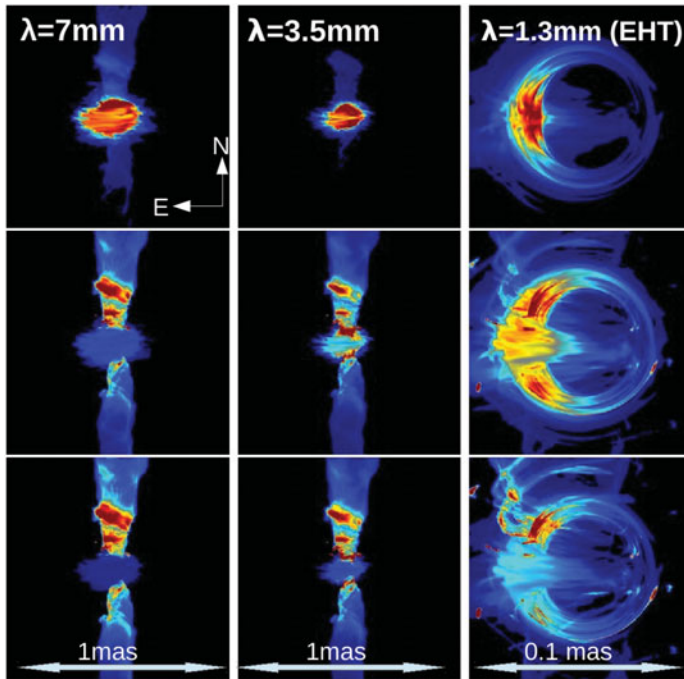
Figure 2. Panels from top to bottom display "infinite"- resolution radio images (synchrotron emission maps) of models with different prescription for the electron temperatures in the accretion disk and the jet. The viewing angle is $i = 90°$. Left, middle, and right columns show the model appearance at $\lambda = 13$, 7 and 1.3 mm, respectively. Colors code the radiation intensity on a linear scale. The field of view of the left and middle panels is $200 \times 200 R_g$ (approximately 1×1 mas), and the right panel's field of view is $20 \times 20 R_g$.

2007, Mościbrodzka et al. 2009, Dexter et al. 2010) and we will call is a single electron temperature model. In the second approach (illustrated in the right panel in Fig. 1), we divide the plasma near the black hole into two regions with different T_e prescription. In the turbulent disk, the electrons are coupled to protons and the coupling is weak, i.e., $C \ll 1$. In the magnetic jet (both in spine and sheath), the electrons have constant temperature. Such assumption is ad hoc but motivated by physical arguments. In the jet the magnetic fields are ordered, anisotropic thermal conduction along the ordered field lines may naturally lead to the isothermal plasma. Enhanced shearing in the jet may also lead to additional kinetic energy dissipation. The second model for T_e, we shall call two-temperature disk plus isothermal jet.

3. Results

3.1. Radio images and spectra as a function of T_e

Fig. 2 shows "infinite"-resolution (i.e., not accounting for interstellar scattering or finite instrumental resolution) synchrotron intensity maps of single GRMHD model time slice, when different electron temperatures are ascribed. The top panels correspond to a single temperature model, while the bottom one to two-temperature disk with isothermal jet. The middle panels show an intermediate case. The models have dramatically different appearances, e.g., at the longest wavelength model with isothermal jet is evidently more extended in comparison to the single temperature model. We found that the model
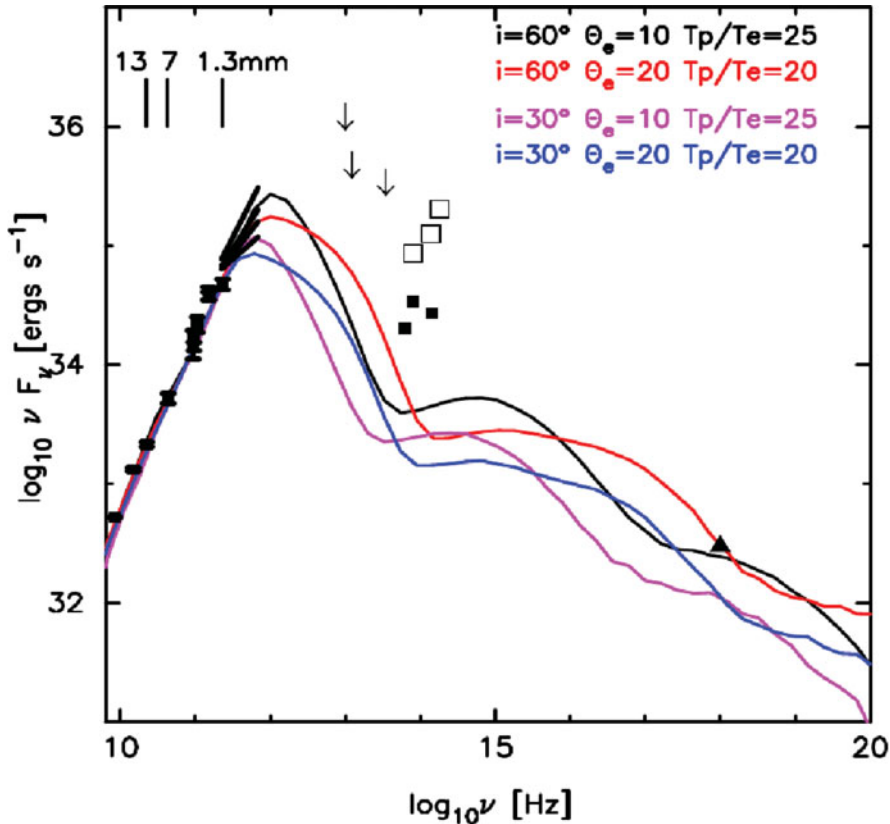
Figure 3. Full SED (including synchrotron and Compton emission) of models which are roughly consistent with the broadband observations of Sgr A* (various models with two-temperature disk plus isothermal jet observed at $i = 60°$ and $30°$). The observational data points and upper limits are taken from Falcke *et al.* (1998), An *et al.* (2005), Marrone *et al.* (2006), Melia & Falcke (2001), Doeleman *et al.* (2008), Schödel *et al.* (2011), and the X-ray luminosity of the inner accretion flow is from Neilsen *et al.* (2013).

size (after convolution with the scattering screen) vs. wavelength relation in the two-temperature disk plus isothermal jet model is consistent with observational constraints. At the shortest wavelength all models become optically thin and the shadow of the black hole horizon is clearly visible. The image of the plasma in the immediate vicinity of the black hole is strongly distorted by the gravitational lensing and Doppler boosting effects.

The same models with the two prescriptions for T_e show dramatic difference in the spectral energy distribution (SED). In particular models with isothermal jets produce radio SEDs that display significantly flatter spectral slopes compared to the single electron temperature model. The model with single temperature plasma shows $\alpha_\nu \approx 2$, but for the two-temperature disk plus isothermal jet model, $\alpha_\nu \approx 0.3$. The nearly flat spectral slope is highly consistent with observed spectrum of Sgr A*. The radio spectral slope weakly depends on the observers viewing angle (Mościbrodzka & Falcke 2013). On the other hand, the X-ray emission, which is formed by the self-synchrotron Compton process in the accretion disk, is sensitive to the viewing angles and put constraints on the inclination angle of the system with respect to the observer.
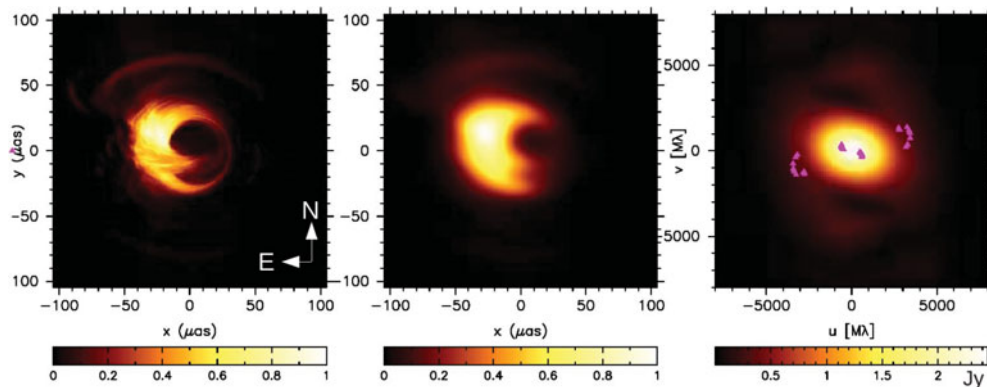
Figure 4. EHT simulated images. Intrinsic image, scatter-broadened image, and visibility amplitude distribution for model with two-temperature disk plus isothermal jet at $\lambda = 1.3$mm. Images are time-averaged (over $\Delta t \approx 3$h) and the color intensity indicates the intensity of radiation normalized to unity (linear scale). The visibility amplitudes are in units of Jansky. The visibility u-v tracks are from Fish *et al.* (2011), and the model is consistent with the EHT detections.

3.2. *Sgr A* SED and synthetic images at $\lambda = 1.3$ mm*

As shown in Fig. 3, the two-temperature plasma with isothermal jet electron temperature prescription naturally describes the observed radio SED of Sgr A*. We found that models with inclinations angles $i \leqslant 60°$ are consistent with radio and X-ray emission observed in Sgr A*.

Fig. 4 displays our "best-bet", the two-temperature disk plus isothermal jet viewed at $i = 60°$, model appearance at EHT wavelength $\lambda = 1.3$ mm (plotted as a red line in Fig. 3). To simulate observations, we convolve the model image with the scattering screen to include the effects of the interstellar medium scatterings. Next, the 2-D power-spectrum of the image (Fourier transformation of the intensity distribution on the sky) is calculated to produce the complex visibility function maps. The synthetic visibility amplitudes are compared to those measured on VLBI baselines between three EHT stations (SMA, SMTO, CARMA) at which Sgr A* has been already detected (Doeleman *et al.* 2008; Fish *et al.* 2011). Our model with two-temperature disk and isothermal jet is fully consistent with these observations. The emitting structure is slightly washed by the scattering effects, but the silhouette of the black hole horizon is visible. The black hole is detectable in the visibility space as two minima located at baselines nearly orthogonal to the currently available ones.

3.3. *Sgr A* geometry at $\lambda = 3.5$mm measured with closure phases*

The intrinsic brightness distribution of Sgr A* at wavelengths longer than EHT $\lambda = 1.3$mm is washed out by the scattering. However, still the intrinsic source geometry could be probed using the visibility (closure) phase information. The closure phase is the VLBI observable that can be measured when the interferometric visibility phases are summed around a triangle of stations. It provides a measure of the ratio of antisymmetric flux density to symmetric flux density as a function of the UV-spacings of the baselines involved.

We carried out a preliminary computations for the expected closure phases evolutions to simulated images of Sgr A* at $\lambda = 3.5$mm according to the two electron temperature prescription models (Brinkerink *et al.* 2014). The observations are simulated using the Very Long Baseline Array (VLBA), augmented by the Green Bank Telescope (GBT) and

the Large Millimeter Telescope (LMT) for increased signal-to-noise ratio. The closure phase time evolution depends on both the model used and the orientation of the source (its inclination and position angle on the sky). We found that the closure phase evolution can be measured with sufficient accuracy using existing facilities to place limits on the orientation and the shape of the source.

4. Summary

Observations of Sgr A* already constrain GRMHD models of accreting black holes. We found that Sgr A* appearance may be well dominated by the emission from the outflowing plasma. The two-temperature disk plus isothermal jet model naturally produces correct slope of the radio SED and its appearance os consistent with the recent EHT observations that estimated the size of the source. The black hole shadow in our "best-bet" model is clearly visible at $\lambda =1.3$ mm.

Current and future mm and sub-mm VLBI observations can probe the geometry of the source even with the smearing by interstellar galactic electrons. However, new generation of GRMHD models with self-consistent electron physics is needed to interpret any observations of Sgr A* (and also M87), to improve our understanding of accretion black holes and how they produce jets.

References

An, T., Goss, W. M., Zhao, J.-H., *et al.* 2005, *ApJL*, 634, L49

Bower, G. C., Falcke, H., Wright, M. C., & Backer, D. C. 2005, *ApJL*, 618, L29

Bower, G. C., Goss, W. M., Falcke, H., Backer, D. C., & Lithwick, Y. 2006, *ApJL*, 648, L127

Bower, G. C., Markoff, S., Brunthaler, A., *et al.* 2014, *ApJ*, 790, 1

Brinkerink, C., Moscibrodzka, M., Fraga-Encinas, R., & Falcke, H., 2014, in preparation

Dexter, J., Agol, E., Fragile, P. C., & McKinney, J. C. 2010, *ApJ*, 717, 1092

Doeleman, S. S., Weintroub, J., Rogers, A. E. E., *et al.* 2008, *Nature*, 455, 78

Doeleman, S. S., Fish, V. L., Schenck, D. E., *et al.* 2012, *Science*, 338, 355

Falcke, H., Goss, W. M., Matsuo, H., *et al.* 1998, *ApJ*, 499, 731

Falcke, H. & Markoff, S. B. 2013, *Classical and Quantum Gravity*, 30, 244003

Fish, V. L., Doeleman, S. S., Beaudoin, C., *et al.* 2011, *ApJL*, 727, L36

Marrone, D. P., Moran, J. M., Zhao, J.-H., & Rao, R. 2006, *ApJ*, 640, 308

Melia, F. & Falcke, H. 2001, *ARAA*, 39, 309

Mościbrodzka, M., Gammie, C. F., Dolence, J. C., Shiokawa, H., & Leung, P. K. 2009, *ApJ*, 706, 497

Mościbrodzka, M. & Falcke, H. 2013, *A&A*, 559, L3

Mościbrodzka, M., Falcke, H., Shiokawa, H., & Gammie, C. F. 2014, *A&A*, 570, AA7

Neilsen, J., Nowak, M. A., Gammie, C., *et al.* 2013, *ApJ*, 774, 42

Noble, S. C., Leung, P. K., Gammie, C. F., & Book, L. G. 2007, *Classical and Quantum Gravity*, 24, 259

Schödel, R., Morris, M. R., Muzic, K., *et al.* 2011, *A&A*, 532, A83